Geoderma 349 (2019) 11–24

Contents lists available at ScienceDirect

Geoderma

journal homepage: www.elsevier.com/locate/geoderma

Projections of future soil temperature in northeast Iran

Alireza Araghi[a,*], Jan Adamowski[b], Christopher J. Martinez[c], Jørgen Eivind Olesen[d]

[a] Department of Water Science and Engineering, Faculty of Agriculture, Ferdowsi University of Mashhad, Mashhad, Iran
[b] Department of Bioresource Engineering, Faculty of Agriculture and Environmental Sciences, McGill University, Sainte-Anne-de-Bellevue, Quebec, Canada
[c] Department of Agricultural and Biological Engineering, Institute of Food and Agricultural Sciences, University of Florida, Gainesville, FL, USA
[d] Department of Agroecology, Aarhus University, Tjele, Denmark

ARTICLE INFO

Handling Editor: Morgan Cristine L.S.

Keywords:
Soil temperature
Projection
STM^2
MarkSim
CMIP5
GCM

ABSTRACT

Soil temperature (*Ts*) is an important meteorological variable that noticeably impacts ecology, agriculture, and hydrology. In contrast to air temperature, there has been little focus on the projection of *Ts* in the future under climate change. In this study, future *Ts* were estimated at three weather stations (Ghoochan, Gonabad and Mashhad) in northeast Iran using an ensemble of 17 General Circulation Models (GCMs) from the Coupled Model Intercomparison Project Phase 5 (CMIP5). These *Ts* were analyzed under different representative concentration pathway (RCP) scenarios by applying the Soil Temperature and Moisture Model (STM^2). For each site, projected estimates were made for 10-year periods between 2025 and 2095, at depths of 5, 10, 20, 50, and 100 cm. Analysis of the data from the three stations yielded *Ts* increments ranging from 0.8 to 1.5 °C, 1.2–2.3 °C, and 2.4–4.4 °C, based on RCP scenarios RCP4.5, RCP6.0 and RCP8.5, respectively. Increased *Ts* may enhance crop development, especially during crop emergence and during parts of the vegetative period, but can also impact soil processes such as the rate of nutrient and CO_2 release from soil organic matter, and the rate of evaporation. Due to this phenomenon, increased *Ts* can create faster and higher water deficits in soil, especially in arid to semi-arid climates. The method used in this study is applicable to diverse geographical contexts and the authors recommend similar studies be undertaken elsewhere in order to obtain further projected *Ts* data. The optimization of the current method may be particularly useful for future agro-climatological studies, as *Ts* impacts both plant and soil processes in addition to soil-atmosphere exchanges.

1. Introduction

Soil temperature (*Ts*) is related to energy balances and thermal exchanges that occur between the soil surface and soil at a given depth. *Ts* is one of the most important variables in agricultural meteorology (Hillel, 1998; Mavi and Tupper, 2004). Many physical, chemical, and biological processes in soil are closely associated with *Ts* (Hillel, 1998) including plant growth and development, root system health, carbon and nitrogen transformations in the soil, and evapotranspiration rate (Allen et al., 1998; Brutsaert, 2010; Mavi and Tupper, 2004). Despite the importance of *Ts*, only a few studies have investigated possible variations in future *Ts* (Bradford et al., 2017; Houle et al., 2012).

In contrast to air temperature (*Ta*) data, which are readily available from various sources such as weather station measurements and gridded datasets (Araghi et al., 2018; Araghi et al., 2015a, b; Fick and Hijmans, 2017), *Ts* records are spatially and temporally limited (Araghi et al., 2017a; Araghi et al., 2017b). This has contributed to the lack of research on *Ts* changes and trends in past decades, even though, in many cases, *Ts* variations are more important than *Ta* fluctuations. This is particularly true for studies in agriculture and ecology (Mavi and Tupper, 2004), since *Ts* significantly influences below ground plant and soil microbial activities, appreciably affecting the carbon cycle (Wisser et al., 2011). An increase in *Ts* may also have considerable effect on CO_2 emissions due to enhanced soil respiration (Crowther et al., 2016; Davidson and Janssens, 2006). Recent studies have observed how over the past decades there have been incremental *Ts* increases across various regions of the world (Araghi et al., 2017a; Fang et al., 2019; Knight et al., 2018; Mellander et al., 2007; Qian et al., 2011). Empirical evidence shows that *Ts* responds to changes in *Ta* in complex ways, depending on the current climatic conditions and soil and vegetation types (Jungqvist et al., 2014; Zhang et al., 2005).

While current research methods (*e.g.,* trend analysis) can be applied to analyze the historical effects of climate change on *Ts*, additional benefits can be acquired by estimating future *Ts* projections (Houle

* Corresponding author.
E-mail addresses: araghi.a@mail.um.ac.ir, alireza_araghi@yahoo.com (A. Araghi), jan.adamowski@mcgill.ca (J. Adamowski), chrisjm@ufl.edu (C.J. Martinez), jeo@agro.au.dk (J.E. Olesen).

https://doi.org/10.1016/j.geoderma.2019.04.034
Received 11 August 2018; Received in revised form 2 April 2019; Accepted 18 April 2019
Available online 02 May 2019

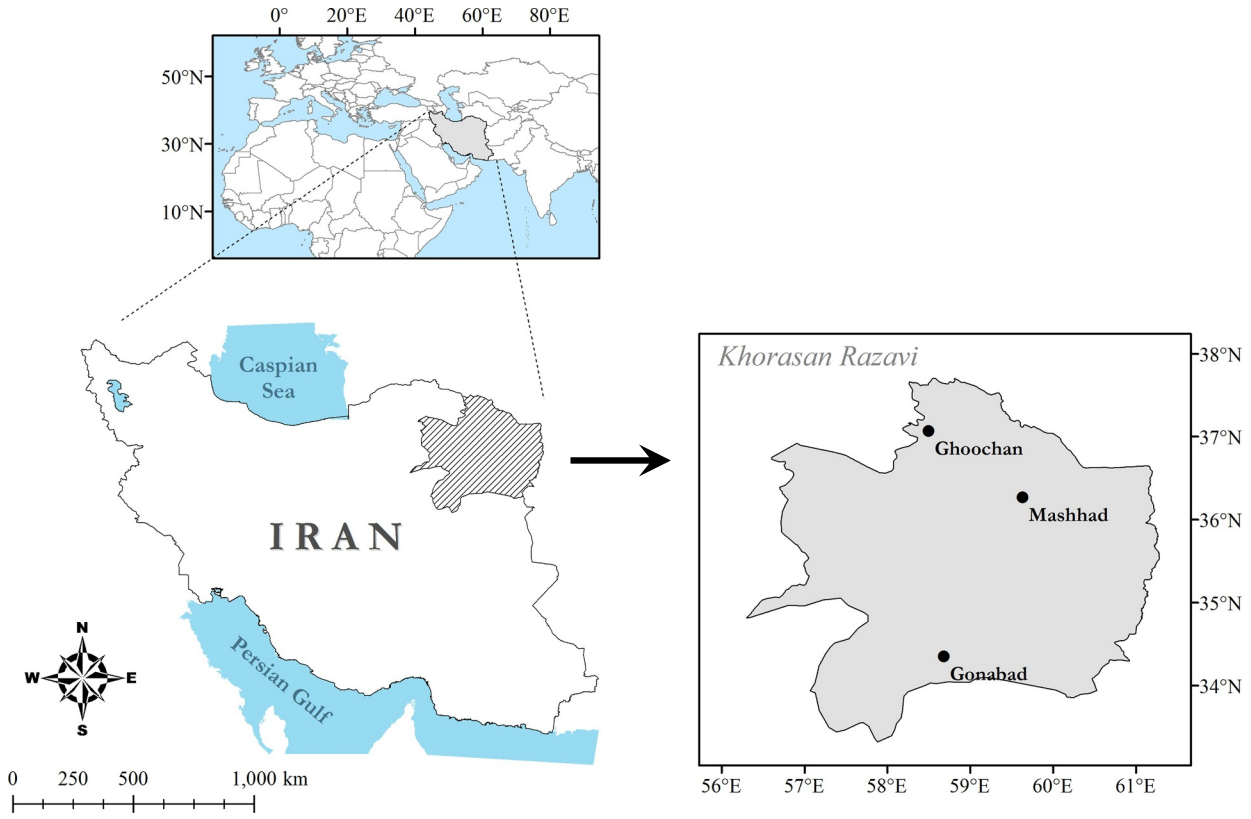

Fig. 1. Location of the selected weather stations in northeast Iran.

Table 1
Geographic characteristics, long-term climatic properties (1993–2017), and soil texture of the studied sites.

Station Name	Longitude (E)	Latitude (N)	Elevation (m)	Annual Total Precipitation (mm)	Annual Mean Temperature (°C)	Fractions of Clay, Silt, Sand (%)	Class of Soil Texture
Ghoochan	58° 30′	37° 04′	1287	315	12.7	30, 34, 35	Clay loam
Gonabad	58° 41′	34° 21′	1056	129	18.6	11, 30, 59	Sandy loam
Mashhad	59° 38′	36° 16′	999.2	242	15.4	21, 44, 35	Loam

et al., 2012). Estimating future *Ts* is useful for planning strategies (*e.g.,* climate change mitigation through soil carbon sequestration) in environmental science and engineering, notably in the agricultural realm (Zhang et al., 2016).

Despite a large volume of research on the future values of many meteorological variables (*e.g.,* temperature and precipitation), very few studies have investigated future projections of *Ts*. Houle et al. (2012) coupled five global climate models and the Forest *Ts* Model (ForSTeM) to project *Ts* up until the year 2100 for three southern Quebec forested sites. Using 30-yr averages (1971–2000), the results of that study showed increases in annual *Ts* between 1.1 and 1.9 °C, and between 1.9 and 3.3 °C, during the periods 2040–69 and 2070–2099, respectively. Batir et al. (2017) used equilibrium temperature-depth measurements from borehole and numerical models based on thermal conductivity in order to study ground surface and subsurface temperatures in northwestern Alaska. They found ground surface temperature to be warming at a rate of ~0.44 ± 0.05 °C/decade, a value consistent with the *Ta* warming of ~1.0 ± 0.8 °C/decade.

There are two major types of models for the estimation of *Ts*: soil physics (or process-based) models and data-driven models. The use of soil physics models is limited because of their large input requirements, from soil physical constants to climatic variables (Flerchinger et al., 1998; Šimůnek et al., 2008). Data-driven models (*e.g.,* artificial neural networks, fuzzy inference systems, and statistical methods) that have been developed for the estimation of *Ts* at different depths and under different climate conditions (Araghi et al., 2017b; Bilgili, 2010; Kemp et al., 1992; Sanikhani et al., 2018; Wu et al., 2013) can be similarly restrictive as they are mostly site-specific and can be used only in the place where they have been developed. It should be noted that the use of physical models, specifically for climate change studies, may be more robust since they are based on a physical understanding of processes in soil.

In the current study, we used downscaled CMIP5 future climate data using a weather generator called MarkSim, and a soil physics model called STM^2 to estimate *Ts* in northeast Iran for the period 2025–2095. Before applying future climate data, the STM^2 model was calibrated and validated using historical data observed at three weather stations. This is the first study that estimated future *Ts* using the method described below.

2. Materials and methods

2.1. Study area and historical data

Iran is located in the Middle East (*i.e.,* southwest Asia) and has an area of about 1.65×10^6 km^2 and a prominent arid and semi-arid climate in most regions (Araghi et al., 2018). The long-term spatio-temporal average annual precipitation in the country is nearly 250 mm year^{-1}; however, it varies from < 50 mm year^{-1} in central parts of the country (*e.g.,* Lut Desert and Central Desert) to > 1500

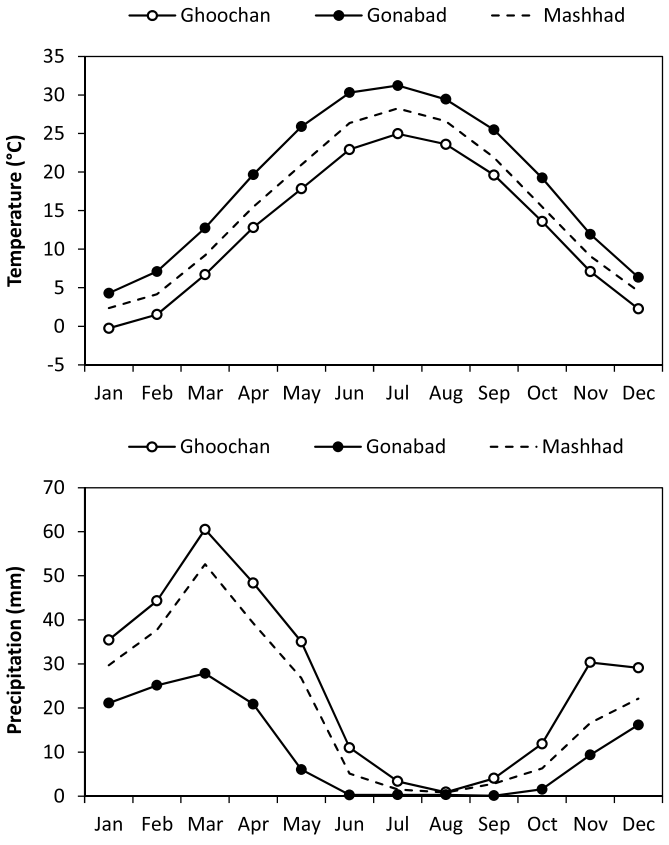

Fig. 2. Long-term monthly average temperature and precipitation at the studied stations from 1993 to 2017.

mm year^{-1} in southern coastal regions of the Caspian Sea. The long-term average annual temperature ranges from < 10 °C in the northwest parts of Iran to > 25 °C in the southwest and southeast (Araghi et al., 2017a).

Iran has 31 provinces and Razavi Khorasan Province, the fifth largest in total area, is in the northeast part of the country. It is one of the most important provinces for agricultural production. Synoptic stations at Ghoochan, Gonabad, and Mashhad in Razavi Khorasan Province were selected for this study (Fig. 1) as they have distinct ranges of climate variables and soil textures (Table 1 and Fig. 2). The climate at these stations is arid and semi-arid — common to most parts of Iran (Araghi et al., 2018). According to World Meteorological Organization (WMO) standards, all of the studied stations are located on 26 × 26 m flat areas (WMO, 2008). The land surface at these stations has no vegetative cover, similar to the surrounding areas, and it receives no irrigation water.

The soil texture values (Table 1) are weighted averages from the surface to a depth of 100 cm (Najafimoud et al., 2008; Perreault et al., 2013). For all stations, soil organic matter levels were < 2% and were mostly observed at shallow depths (*i.e.,* < 10 cm). Soil texture and organic matter at all three stations were representative of the study sites. Following WMO standards, a bare patch of ground (4 × 6 m) in the southeastern part of each station enclosure has been reserved for observations of *Ts* at depths of 5 to 100 cm, three times a day, at 03, 09, and 15 GMT (*i.e.,* Greenwich Mean Time), using mercury-in-glass thermometers. For *Ts* measurements at depths of 5–30 cm, the thermometer with its stem bent at a right angle is installed into the ground and is read without removing. For depths of 50 and 100 cm, straight thermometers are installed underground and are removed and replaced for each observation. Thermometers of 50 and 100 cm are placed in a special pipe-shaped shield (Araghi et al., 2017b; WMO, 2008). Synoptic stations across the country are operated by the Iran Meteorological Organization (IRIMO). Climate data from the stations at Ghoochan, Gonabad, and Mashhad are available beginning in 1984, 1987, and 1951, respectively. The collection of *Ts* data began in June 1992 at all of Iran's synoptic stations.

2.2. Future projected climate data and downscaling

For this study, two sets of data were used: i) historical daily *Tx*, *Tm*, *P*, and *Ts* data at depths of 5, 10, 20, 50, and 100 cm, from each of the three weather stations, and ii) future projections of downscaled climate data based on the fifth phase of the Coupled Model Intercomparison Project (CMIP5) using the MarkSim application.

CMIP5 includes long-term simulations of the climate of the twentieth-century and projections for the twenty-first century (IPCC, 2013; Taylor et al., 2012). CMIP5, a state-of-the-art multi-model dataset, was designed to improve knowledge of climate variability and climate change, particularly for future decades (IPCC, 2013). There are several General Circulation Models (GCM) in the CMIP5 project under a range

Table 2
General circulation models (GCMs) used in the current study.

No.	Model	Institution	Resolution Lat × Long °	Reference
1	BCC-CSM 1.1	Beijing Climate Center, China Meteorological Administration	2.8125 × 2.8125	(Wu, 2012)
2	BCC-CSM 1.1(m)	Beijing Climate Center, China Meteorological Administration	2.8125 × 2.8125	(Wu, 2012)
3	CSIRO-Mk 3.6.0	Commonwealth Scientific and Industrial Research Organization and the Queensland Climate Change Centre of Excellence	1.875 × 1.875	(Collier et al., 2011)
4	FIO-ESM	The First Institute of Oceanography, SOA, China	2.812 × 2.812	(Song et al., 2012)
5	GFDL-CM3	Geophysical Fluid Dynamics Laboratory	2.0 × 2.5	(Donner et al., 2011)
6	GFDL-ESM2G	Geophysical Fluid Dynamics Laboratory	2.0 × 2.5	(Dunne et al., 2012)
7	GFDL-ESM2M	Geophysical Fluid Dynamics Laboratory	2.0 × 2.5	(Dunne et al., 2012)
8	GISS-E2-H	NASA Goddard Institute for Space Studies	2.0 × 2.5	(Schmidt et al., 2006)
9	GISS-E2-R	NASA Goddard Institute for Space Studies	2.0 × 2.5	(Schmidt et al., 2006)
10	HadGEM2-ES	Met Office Hadley Centre	1.2414 × 1.875	(Collins et al., 2011)
11	IPSL-CM5A-LR	Institute Pierre-Simon Laplace	1.875 × 3.75	(Dufresne et al., 2013)
12	IPSL-CM5A-MR	Institute Pierre-Simon Laplace	1.2587 × 2.5	(Dufresne et al., 2013)
13	MIROC-ESM	Atmosphere and Ocean Research Institute (The University of Tokyo), National Institute for Environmental Studies, and Japan Agency for Marine-Earth Science and Technology	2.8125 × 2.8125	(Watanabe et al., 2011)
14	MIROC-ESM-CHEM	Atmosphere and Ocean Research Institute (The University of Tokyo), National Institute for Environmental Studies, and Japan Agency for Marine-Earth Science and Technology	2.8125 × 2.8125	(Watanabe et al., 2011)
15	MIROC5	Japan Agency for Marine-Earth Science and Technology, Atmosphere and Ocean Research Institute (The University of Tokyo), and National Institute for Environmental Studies	1.4063 × 1.4063	(Watanabe et al., 2010)
16	MRI-CGCM3	Meteorological Research Institute	1.125 × 1.125	(Yukimoto et al., 2012)
17	NorESM1-M	Norwegian Climate Centre	1.875 × 2.5	(Kirkevag et al., 2008), (Seland et al., 2008)

Table 3
Brief explanations of the four RCP scenarios (IPCC, 2013; Moss et al., 2010; Rogelj et al., 2012).

Scenario	Radiative forcing	CO_2 equivalent (ppm)	Air temperature increase above pre-industrial (°C)	Pathway
RCP8.5	> 8.5 $W{\cdot}m^{-2}$ in 2100	> 1370 in 2100	~4.9	Rising
RCP6.0	~6 $W{\cdot}m^{-2}$ after 2100	~850 after 2100	~3.0	Stabilization without overshoot
RCP4.5	~4.5 $W{\cdot}m^{-2}$ after 2100	~650 after 2100	~2.4	Stabilization without overshoot
RCP2.6	Peak at ~3 $W{\cdot}m^{-2}$ before 2100, decreasing to ~2.6 $W{\cdot}m^{-2}$ by 2100	~490 before 2100, decreasing after 2100	~1.5	Peak and decline

of representative concentration pathways (RCPs), presented by different atmospheric-oceanic research centers worldwide. These RCPs are named after a range of radiative forcing values predicted for the year 2100 relative to pre-industrial values, +2.6, +4.5, +6.0, and + 8.5 W/m^2, respectively (IPCC, 2013). The RCP scenarios are defined based on the range of possible changes in future anthropogenic greenhouse gas (GHG) emissions and their atmospheric concentrations. The RCPs integrate different future emission scenarios for CO_2, CH_4, N_2O, O_3, and other GHGs, and calculate the CO_2 equivalent of these GHGs (Meinshausen et al., 2011; Moss et al., 2010). The peaks of greenhouse gas emissions in scenarios RCP2.6, RCP4.5, and RCP6.0 are estimated to occur between 2010 and 2020, 2040, and 2080, respectively (IPCC, 2013; Taylor et al., 2012). More details about the RCP scenarios are presented in Table 3. In addition, each of the four RCPs: RCP2.6, RCP4.5, RCP6.0, and RCP8.5, were used for future weather data generation.

In this study, the MarkSim weather generator (Jones and Thornton, 2000) was employed to prepare input variables for the STM^2 model in order to estimate future *Ts*. This application was originally designed for use with the decision support system for agrotechnology transfer (DSSAT), and its current version can generate future daily weather data based on 17 GCMs from the CMIP5 project (Table 2) under different RCPs (Jones and Thornton, 2015). Each of these GCMs was developed and run by major atmospheric-oceanic research centers around the world. An ensemble of all 17 GCMs available in the MarkSim was used in this research to downscale and generate future *Tx*, *Tm*, and *P* from 2025 to 2095 with a 10-year interval for the selected stations (Table 1). It should be noted that using a multi-GCM ensemble (as was done in this study), instead of employing just a single GCM, is a commonly used method to reduce inherent uncertainties within the GCMs in order to have more robust climatic values for future periods (IPCC, 2013; Pierce et al., 2009).

The MarkSim produces 0.5° × 0.5° grid resolution data from the GCMs coarse resolution outputs using stochastic downscaling and climate typing techniques. It has been calibrated for over 10,000 stations worldwide (Jones and Thornton, 2013; Jones and Thornton, 2015) including Razavi Khorasan Province, where it was evaluated and performed well (Paymard et al., 2018). The MarkSim generates daily rainfall data based on a third-order Markov stochastic model (Jones and Thornton, 2013), and applies Richardson's methods for estimating daily *Tx* and *Tm* as well as daily solar radiation (Richardson, 1981). For any location, MarkSim needs a climate record including longitude, latitude, elevation, monthly mean values of rainfall, daily average temperature, and diurnal variation of temperature. After preparing this climate record for a standard date using the 12-point Fast Fourier transform, the estimated GCM differential values are added to estimate future climate data. Note that the GCMs are previously downscaled to 0.5° × 0.5° using conservative remapping, which maintains the global averages. According to the geographical location of any site identified for MarkSim, it uses the nearest grid points from the downscaled CMIP5 ensemble models for estimating future climate at the study site. More details about the downscaling process can be found in Jones and Thornton (2013).

In this study, the number of replications in the MarkSim was set to 99, the maximum possible value. This means that the MarkSim generated 99 stochastic daily time series for each variable in each year based on the selected RCP and GCMs. For instance, MarkSim generated 99 daily *Tx* time series for the year 2045 under the RCP6.0 scenario at Mashhad station based on an ensemble of 17 GCMs. Then, these 99 time series of each variable, year, RCP scenario, and station, were averaged before applying them to the STM^2. This process can lessen the variability produced by a weather generator (Apipattanavis et al., 2007; Peleg et al., 2017). Projected future changes in mean annual temperature and precipitation (relative to 1993–2017), based on the ensemble of 17 GCMs, and under the different RCP scenarios in the studied stations, are presented in Fig. 3.

Table 4
Performance evaluation of the STM^2 model for 2014 before and after applying the bias correction (BC) methods at the Ghoochan station (LR: linear regression, QR: quadratic regression, LS: linear scaling, VARI: variance scaling, DM: distribution mapping).

Depth (cm)	BC method	RMSE (°C)	MAE (°C)	MAPE (%)	R^2
5	No BC	3.2	2.5	172.6	0.95
	LR	2.6	2.0	114.3	0.95
	QR	2.1	1.7	96.8	0.96
	LS	2.1	1.6	103.5	0.96
	VARI	2.0	1.6	62.0	0.97
	DM	2.5	1.9	109.2	0.95
10	No BC	3.3	2.9	115.4	0.96
	LR	2.0	1.5	52.0	0.96
	QR	1.6	1.2	54.2	0.98
	LS	1.7	1.2	48.8	0.97
	VARI	1.6	1.2	39.6	0.98
	DM	2.0	1.4	47.8	0.96
20	No BC	2.4	1.9	135.9	0.98
	LR	1.5	1.0	104.6	0.96
	QR	1.2	0.8	73.0	0.99
	LS	1.1	0.7	76.9	0.99
	VARI	1.2	1.0	41.2	0.99
	DM	1.5	1.0	104.7	0.98
50	No BC	2.9	2.3	37.5	0.96
	LR	1.9	1.3	24.0	0.96
	QR	1.7	1.3	19.9	0.97
	LS	1.1	0.8	13.2	0.98
	VARI	1.2	0.9	11.6	0.98
	DM	1.9	1.3	23.9	0.96
100	No BC	3.7	3.3	34.2	0.90
	LR	2.3	1.9	18.7	0.90
	QR	2.1	1.8	16.7	0.91
	LS	1.0	0.8	7.2	0.98
	VARI	1.1	0.8	7.8	0.98
	DM	2.3	1.9	19.3	0.90

Table 5-
Performance evaluation of the STM^2 model for 2014 before and after applying the bias correction (BC) methods at the Gonabad station (LR: linear regression, QR: quadratic regression, LS: linear scaling, VARI: variance scaling, DM: distribution mapping).

Depth (cm)	BC method	RMSE (°C)	MAE (°C)	MAPE (%)	R^2
5	No BC	3.2	2.6	20.1	0.98
	LR	2.0	1.5	29.5	0.98
	QR	1.7	1.4	17.0	0.98
	LS	1.4	1.1	15.3	0.99
	VARI	1.8	1.4	11.8	0.98
	DM	2.0	1.5	30.7	0.98
10	No BC	2.7	2.3	15.9	0.98
	LR	1.6	1.2	14.3	0.98
	QR	1.3	1.0	9.9	0.99
	LS	1.1	0.8	8.2	0.99
	VARI	1.5	1.1	8.4	0.99
	DM	1.6	1.2	14.6	0.98
20	No BC	2.6	2.1	13.0	0.99
	LR	1.3	1.1	9.0	0.99
	QR	1.2	1.0	7.9	0.99
	LS	1.0	0.8	5.8	0.99
	VARI	1.3	1.0	6.9	0.99
	DM	1.3	1.1	9.2	0.99
50	No BC	3.8	3.3	14.8	0.96
	LR	2.1	1.7	10.4	0.96
	QR	2.0	1.7	10.3	0.96
	LS	1.3	1.0	6.0	0.99
	VARI	1.5	1.2	7.0	0.99
	DM	2.1	1.7	10.6	0.96
100	No BC	5.3	4.3	17.0	0.93
	LR	2.0	1.7	9.2	0.93
	QR	2.0	1.7	9.0	0.93
	LS	0.8	0.6	3.2	0.99
	VARI	0.9	0.7	3.7	0.99
	DM	2.0	1.8	9.3	0.93

Table 6
Performance evaluation of the STM^2 model for 2014 before and after applying the bias correction (BC) methods at the Mashhad station (LR: linear regression, QR: quadratic regression, LS: linear scaling, VARI: variance scaling, DM: distribution mapping).

Depth (cm)	BC method	RMSE (°C)	MAE (°C)	MAPE (%)	R^2
5	No BC	2.6	2.0	35.8	0.97
	LR	2.0	1.5	31.1	0.97
	QR	1.7	1.3	22.1	0.98
	LS	1.6	1.2	24.4	0.98
	VARI	1.8	1.4	22.4	0.98
	DM	2.1	1.5	33.0	0.97
10	No BC	2.9	2.5	36.3	0.98
	LR	1.6	1.1	26.5	0.98
	QR	1.4	1.1	20.2	0.99
	LS	1.3	1.0	20.9	0.99
	VARI	1.5	1.2	18.6	0.98
	DM	1.6	1.1	27.3	0.98
20	No BC	2.3	2.0	25.5	0.99
	LR	1.2	0.8	28.3	0.99
	QR	1.1	0.8	21.9	0.99
	LS	1.0	0.7	19.8	0.99
	VARI	1.3	1.1	13.4	0.99
	DM	1.2	0.8	29.1	0.99
50	No BC	2.1	1.6	15.9	0.97
	LR	1.5	1.1	10.1	0.97
	QR	1.5	1.1	9.7	0.98
	LS	1.0	0.8	6.7	0.99
	VARI	1.2	0.9	7.3	0.99
	DM	1.5	1.2	10.5	0.97
100	No BC	2.9	2.5	14.8	0.95
	LR	1.6	1.3	9.0	0.95
	QR	1.6	1.3	8.8	0.95
	LS	0.7	0.6	3.8	0.99
	VARI	0.8	0.6	4.4	0.99
	DM	1.6	1.4	9.4	0.95

2.3. Model for estimating Ts

In this study, a model called the Soil Temperature and Moisture Model (STM^2), developed by the United States Department of Agriculture, Agricultural Research Service (USDA ARS), was employed (Spokas and Forcella, 2009). Empirical and physical models are used in STM^2 to estimate fundamental soil physical parameters and improve the usability of the model by keeping required inputs to a minimum. Using this approach, input requirements of the STM^2 model are limited to daily maximum and minimum temperature (*Tx*, *Tm*), precipitation (*P*), as well as some rudimentary soil properties (*e.g.*, soil texture and organic matter). Using these inputs the model can generate *Ts* and moisture at different depths and several different time intervals (Spokas and Forcella, 2009). The applicability of the STM^2 model has been verified by Perreault et al. (2013), and its results, especially for *Ts*, have been reliable (Perreault et al., 2013; Spokas and Forcella, 2009). The STM^2 model was downloaded from https://www.ars.usda.gov/research/software/download/?softwareid=209.

Various parameters must be set before the STM^2 model can be run. The STM^2 is not a multilayer model and assumes soil properties to be homogenous throughout the soil profile being simulated. Therefore, the weighted average of soil texture from the surface to a depth of 100 cm was used for each site (see Table 1). The climate class in the STM^2 was set to arid to match the arid and semi-arid climate of the study area. The long-term average wind speed at all stations was between 6 and 10 $km \cdot h^{-1}$, and therefore the average wind speed was set to light breeze. The model's default values of −500 and −200 kPa were used as the soil moisture lower boundary condition and initial water potential, respectively. The mean annual *Ta* was set as the lower temperature boundary condition (Perreault et al., 2013). The options of solar heating, evaporation, evaporation scaled by humidity, and snow melt, were enabled (as default), and the fraction of runoff was set to the default value of 50%.

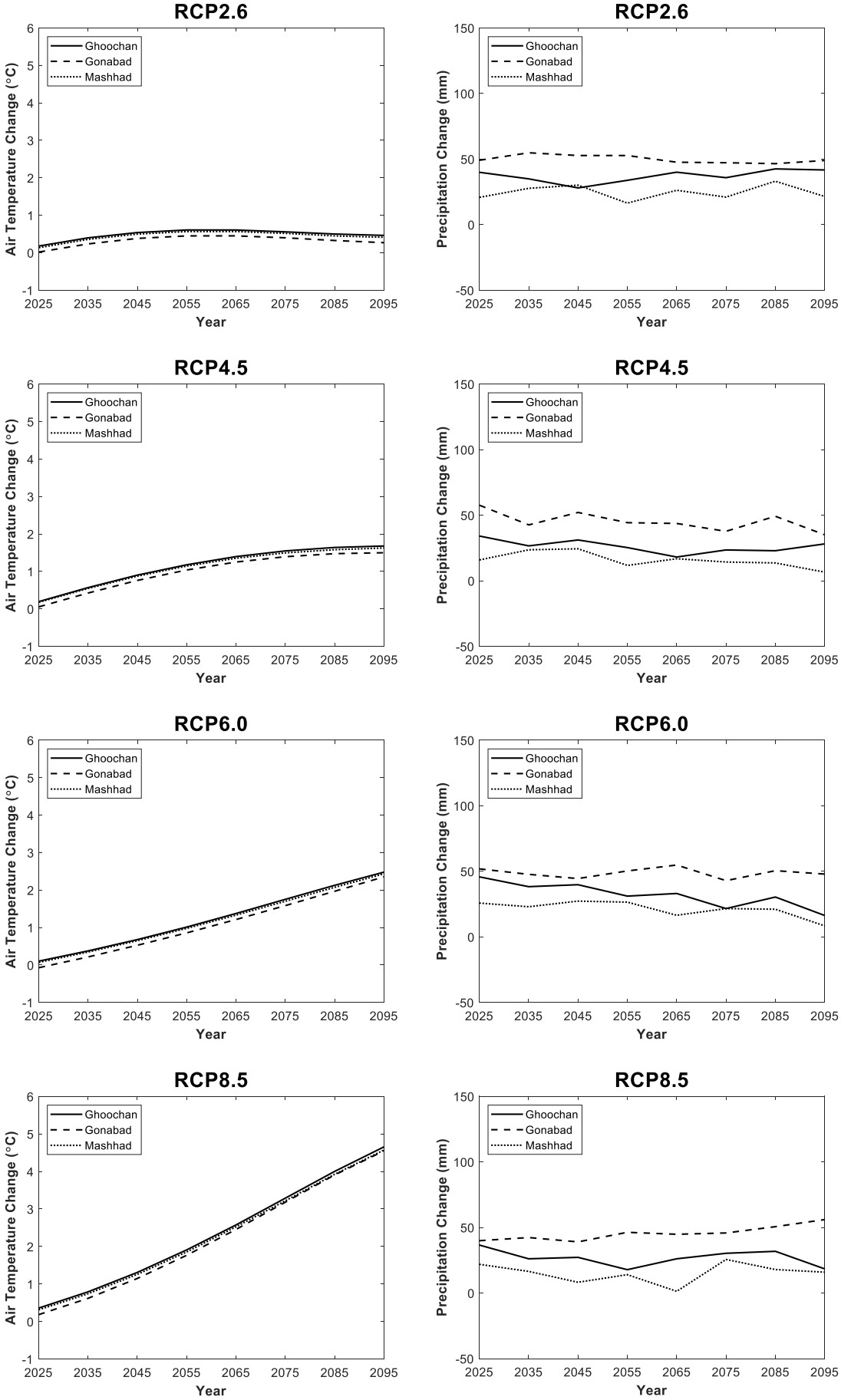

Fig. 3. Future changes for temperature and precipitation compared to a past period (1993–2017), applying an ensemble of 17 GCMs under different RCP scenarios in the studied weather stations.

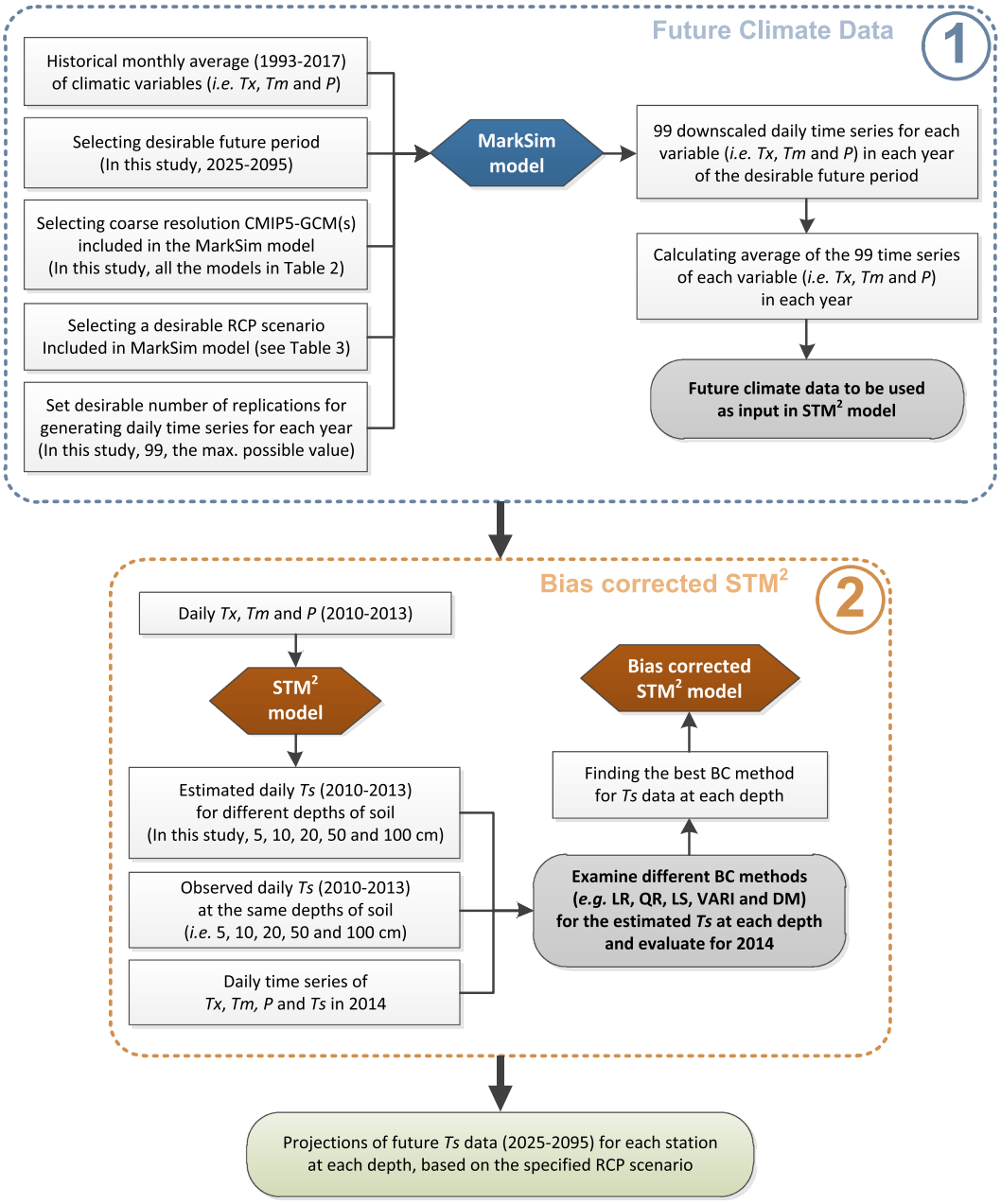

Fig. 4. Schematic diagram of workflow used in the current study (BC: bias correction, *Tx*: maximum air temperature, *Tm*: minimum air temperature, *Ts*: soil temperature, *P*: precipitation) (Note: The steps in Box 1 were repeated for each station and each RCP scenario, and the steps in Box 2 were repeated for each station and each depth of soil).

2.4. Bias correction of the STM^2 outputs

To reduce uncertainties related to the STM^2 model for estimated future *Ts*, bias correction (BC) was performed on the STM^2 outputs before applying future climate data to the model. For this purpose, the STM^2 model was first applied to weather data from 2010 to 2013 at each of the selected stations to estimate *Ts* at different depths. Then different BC methods were employed using estimated and observed *Ts* data over 2010–2013, followed by evaluation using data from 2014. Accordingly, the best BC method for each station at each depth of soil was chosen based on three criteria, namely root mean square error (RMSE), mean absolute error (MAE), and mean absolute percentage error (MAPE), as follows (Hyndman and Koehler, 2006):

$$e_i = O_i - M_i \quad (1)$$

$$p_i = 100\,\frac{e_i}{M_i} \quad (2)$$

$$RMSE = \sqrt{\frac{1}{N}\sum_{i=1}^{N} e_i^2} \quad (3)$$

$$MAE = \frac{1}{N}\sum_{i=1}^{N} |e_i| \quad (4)$$

$$MAPE = \frac{1}{N}\sum_{i=1}^{N} |p_i| \quad (5)$$

where O_i, M_i, N, e_i, and p_i are the observed data, model outputs, length of data, model error, and percentage error, respectively.

2.4.1. Linear regression (LR)

LR is one of the most widely used methods for detecting relations between two different variables, and also for BC purposes (Piani et al., 2010; Wilks, 2011). It is defined as (Chatterjee and Hadi, 2012):

$$O = \beta_0 + \beta_1 M \tag{6}$$

$$M_{cor} = \widehat{\beta}_0 + \widehat{\beta}_1 M \tag{7}$$

where O, M, and M_{cor} are the observed data, STM^2 model outputs, and BC model outputs, respectively. β_0 and β_1 are the regression coefficients and $\widehat{\beta}_0$ and $\widehat{\beta}_1$ are the least squares estimates of β_0 and β_1 (Chatterjee and Hadi, 2012).

2.4.2. Quadratic regression (QR)

QR is very similar to LR. Both are linear methods as the regression coefficients enter the equation linearly (Chatterjee and Hadi, 2012):

$$O = \beta_0 + \beta_1 M + \beta_2 M^2 \tag{8}$$

$$M_{cor} = \widehat{\beta}_0 + \widehat{\beta}_1 M + \widehat{\beta}_2 M^2 \tag{9}$$

wherein the terms in Eqs. (8) and (9) are the same as Eqs. (6) and (7).

2.4.3. Linear scaling (LS)

The LS method uses a constant correcting coefficient which is estimated by the difference between observed and modeled data for each month (Lenderink et al., 2007):

$$M_{cor,m,d} = M_{m,d} + [\,\mu(O_m) - \mu(M_{\mathrm{m}})\,] \tag{10}$$

where $M_{cor,m,d}$ and $M_{m,d}$ are the corrected and original outputs of the STM^2 model on the dth day of the mth month, respectively. Also, $\mu(O_m)$ and $\mu(M_m)$ are the mean of observed and modeled data on the mth month, respectively.

2.4.4. Variance scaling (VARI)

The VARI method was proposed to correct both the mean and variance of any variable with normal distribution such as temperature (Leander and Buishand, 2007):

$$M_{cor,m,d} = [\,M_{m,d} - \mu(M_m)\,] \times \frac{\sigma(O_m)}{\sigma(M_m)} + \mu(O_m) \tag{11}$$

where $\sigma(.)$ denotes the standard deviation. The other terms are the same as those explained for Eq. (10).

2.4.5. Distribution mapping (DM)

In the DM method, the cumulative distribution function (CDF) of the modeled data is matched to the CDF of the observed data (Ines and Hansen, 2006; Piani et al., 2010). As the Normal probability density function (PDF) is well fitted on temperature, it is commonly selected in the DM method for application on temperature data (Teutschbein and Seibert, 2012):

$$f_N(x|\,\mu,\sigma) = \frac{1}{\sigma\sqrt{2\pi}} e^{\frac{-(x-\mu)^2}{2\sigma^2}};\ x \in \mathbb{R} \tag{12}$$

$$M_{cor,m,d} = F_N^{-1}(F_N(M_{m,d}\,|\,\mu(M_m),\sigma(M_m))\,|\,\mu(O_m),\sigma(O_m)) \tag{13}$$

where $f_N(.)$, $F_M(.)$, and $F_O{}^{-1}(.)$ are the Normal PDF, CDF, and its inverse, respectively. The other terms are the same as those explained in previous equations.

2.5. Application of future climate data to the soil model

After detecting the best BC method for the estimated *Ts* data at each depth of soil at each station, the future climate data (generated by MarkSim) were applied as inputs to the STM^2 model. Finally, the future *Ts* values estimated by the STM^2 model were bias-corrected using the best BC method (according to each depth of soil and each station). These corrected *Ts* values were analyzed to estimate future *Ts* changes based on different RCPs, relative to the available *Ts* records from 1993 to 2017. A summarized flowchart of the methodology is presented in Fig. 4.

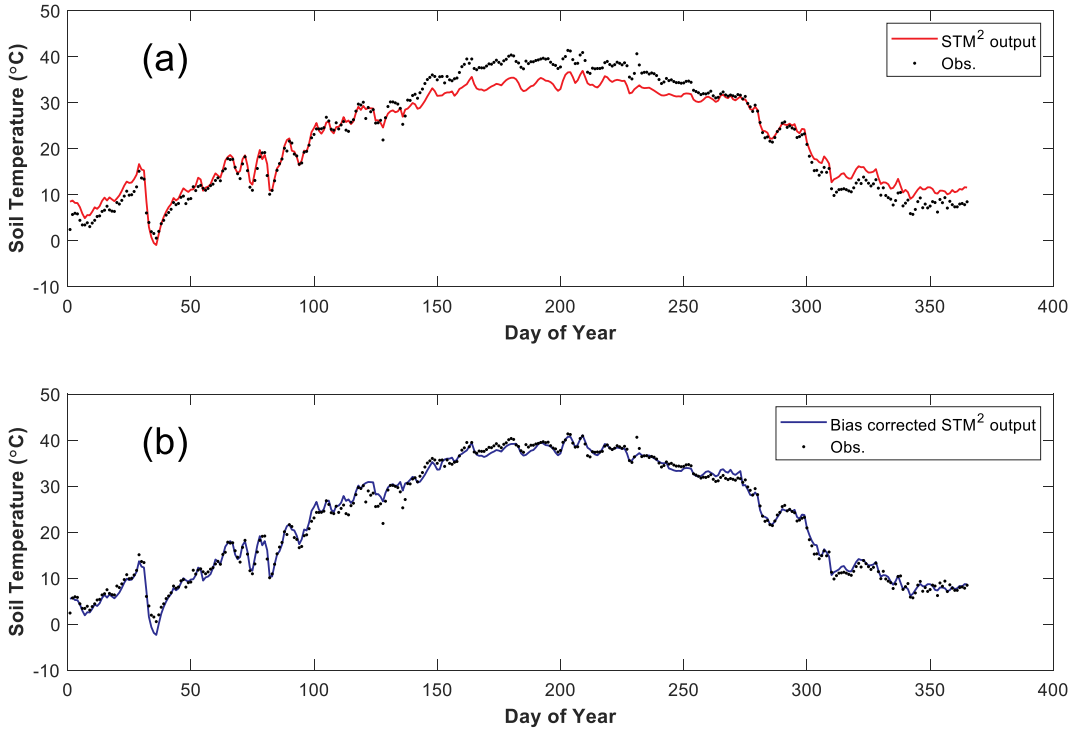

Fig. 5. Observed and estimated soil temperature at a depth of 10 cm in the year 2014 at Gonabad station, before (a) and after (b) bias correction using the linear scaling (LS) method.

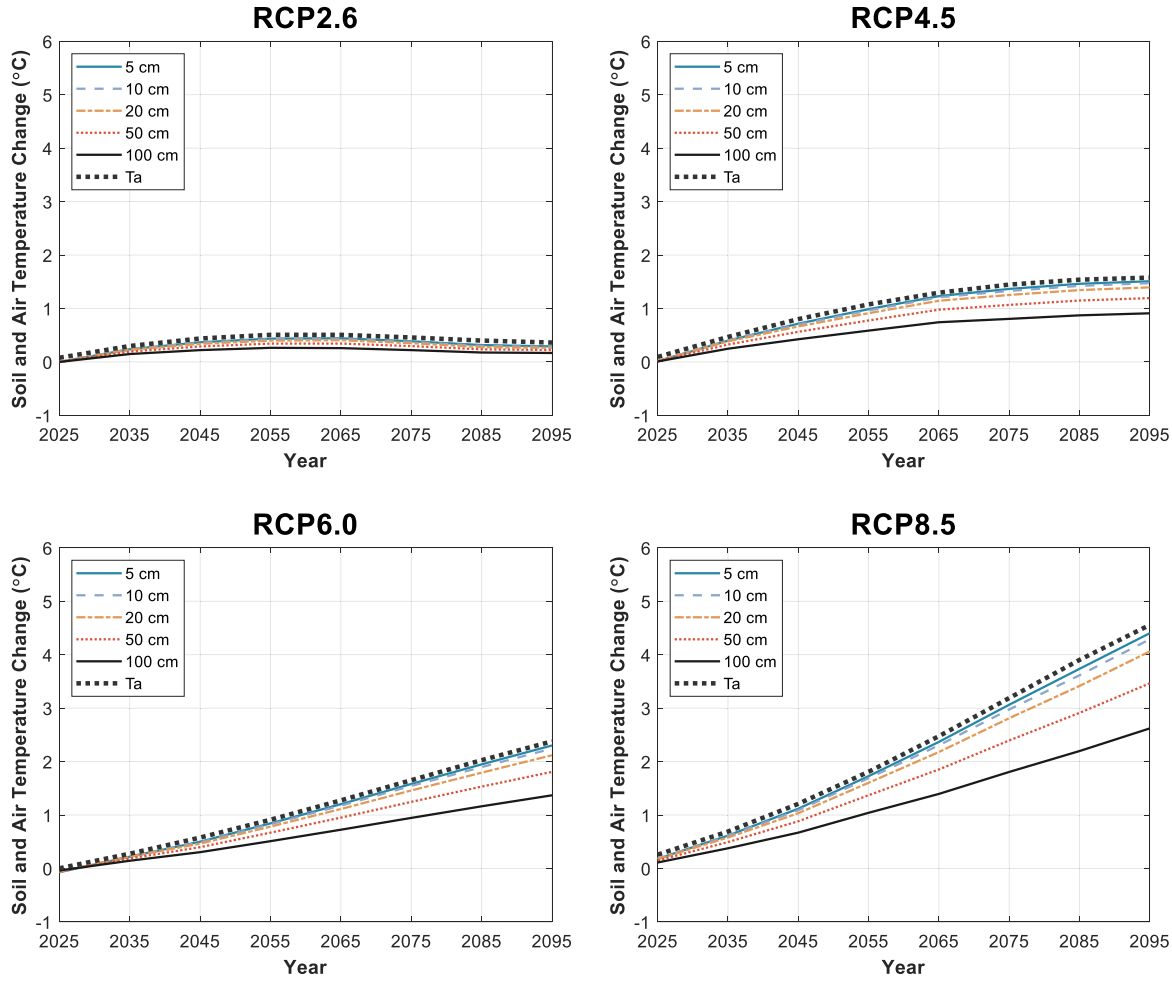

Fig. 6. Changes to future *Ts* and *Ta* projections at Ghoochan station as compared to the period of 1993–2017. Determined using 17 General Circulation Models (GCMs) under four representative concentration pathways (RCPs) and the soil temperature and moisture model (STM^2).

3. Results and discussion

3.1. Evaluation of the STM^2 model

The results in Tables 4–6 revealed detectable improvements in the STM^2 model outputs after BC at all three stations at all depths, although the model's original outputs (with no BC) had suitable accuracy as verified in previous studies (Perreault et al., 2013). The RMSE showed a performance improvement of > 1 °C in most cases and exhibited a range of 2.1–5.3 °C and 0.7–2.0 °C, before and after BC, respectively. As can be seen in Tables 4–6, the VARI was only determined to be the best BC method (with a slight difference in results from LS) at depths of 5 and 10 cm at Ghoochan station, while in all other cases LS was the best BC method. The lowest RMSE values after BC were found at a depth of 100 cm in all studied stations, while the RMSE values were the highest at this depth before BC.

Detecting the LS as the best BC method indicated that the STM^2 model performed well when estimating daily variations of *Ts*, as the LS method only corrected bias for the means of the data (see Section 2.4.3). If the estimated and observed data had different means and standard deviations, the VARI would have been the best BC method (Leander and Buishand, 2007). In most cases, the VARI and QR were the best BC methods after LS, while the LR and DM methods had similar results (Tables 4–6). For instance, the estimated *Ts* with the STM^2 model before and after BC at a depth of 10 cm at the Gonabad station in 2014 is presented in Fig. 5. It is clear in this figure that the LS method significantly reduced biases between estimated and observed values.

3.2. Changes of Ts in future decades

Projections for *Ts* change in future decades based on different RCP scenarios for the studied stations are presented in Figs. 6–8. Under the RCP2.6 scenario, an increase of < 0.5 °C by 2095 was predicted for *Ts* in all of the studied stations. Under the RCP4.5 scenario, *Ts* changes ranged from 1 to 1.5 °C, 0.8–1.4 °C, and 0.9–1.5 °C, by 2095, at the Ghoochan, Gonabad, and Mashhad stations, respectively. *Ts* changes under the RCP6.0 scenario by the year 2065 were comparable to those under the RCP4.5 scenario at all stations. After 2065, this order changed and *Ts* under the RCP6.0 scenario increased significantly more than under RCP4.5. *Ts* changes under the RCP6.0 scenario ranged from 1.3 to 2.3 °C, 1.2–2.2 °C, and 1.2–2.2 °C, by 2095 in the Ghoochan, Gobanad and Mashhad stations, respectively (Fig. 6–8). The maximum *Ts* changes by the year 2095 at all of the studied stations were observed under the RCP8.5 scenario, ranging from 2.6 to 4.4 °C, 2.4–4.2 °C, and 2.5–4.2 °C for the Ghoochan, Gonabad, and Mashhad stations, respectively. Given the different soil textures in the studied stations, it seems that long-term future *Ts* changes are not noticeably influenced by soil texture, although this would need to be further confirmed by similar studies in other regions.

As can be seen in Figs. 6–8, *Ts* increments varied directly with

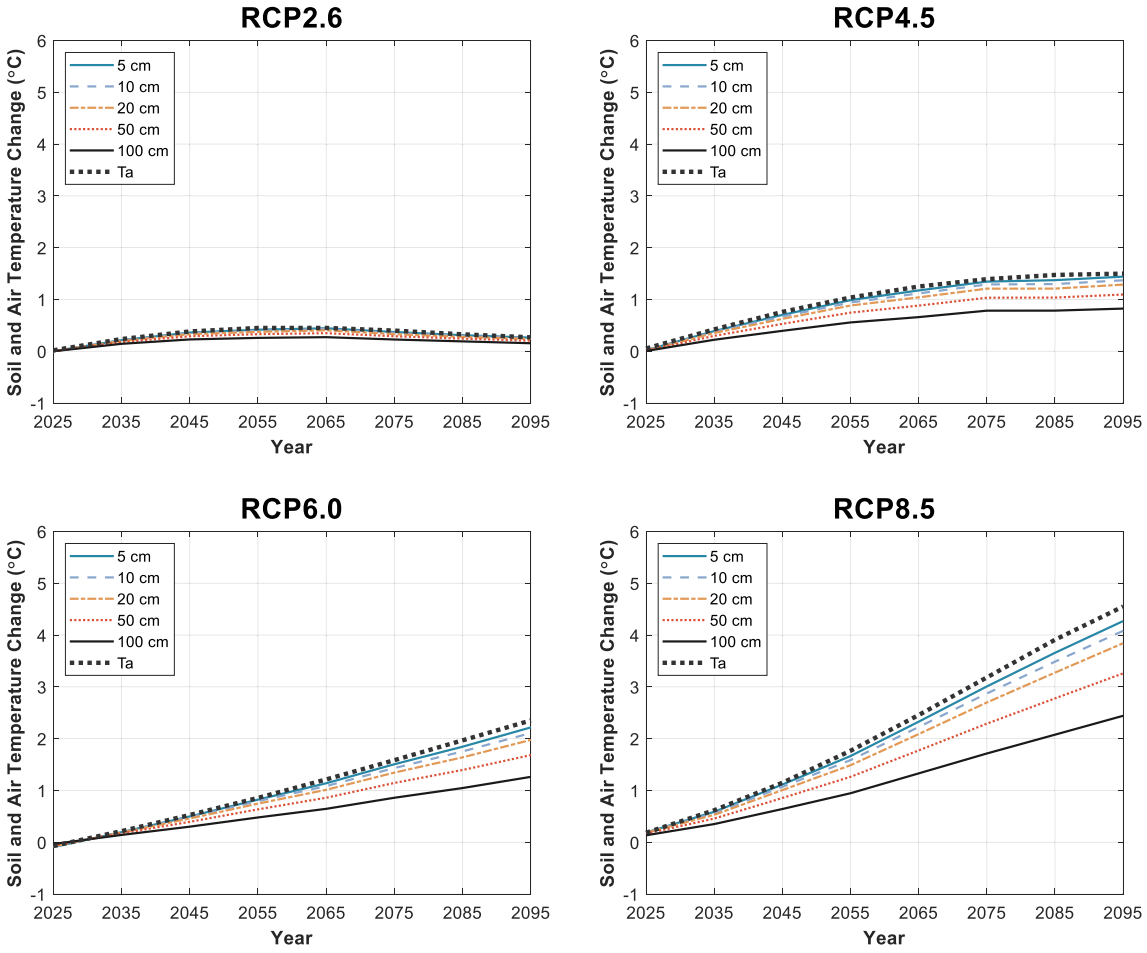

Fig. 7. Changes to future *Ts* and *Ta* projections at Gonabad station as compared to the period of 1993–2017. Determined using 17 General Circulation Models (GCMs) under four representative concentration pathways (RCPs) and the soil temperature and moisture model (STM^2).

depth, so that the highest *Ts* increments corresponded with the shallowest depth (5 cm), and the lowest increments were predicted at the deepest depth (100 cm). Moreover, differences between the highest and lowest *Ts* changes (*i.e.,* at depths of 5 and 100 cm) by the year 2095 increased from RCP2.6 to RCP8.5. This may be linked to the theory that *Ts* in deeper layers of soil is less related to atmospheric changes, and more influenced by heat fluxes through the soil from surface to deeper layers (Hillel, 1998).

Comparing future trends of *Ta* and *Ts* revealed that changes in *Ts*, particularly at shallow depths, were almost the same as *Ta* at all studied stations. Trends for future *Ts* changes in deeper layers of soil, especially between 50 and 100 cm, had the lowest similarity with *Ta*. This may be related to higher correlations between *Ta* and *Ts* at shallow depths, a common correlation in most regions (Araghi et al., 2017a; Araghi et al., 2017b; Hillel, 1998). Correlations between *Ta* and *Ts* at different depths of soil over several historical periods are illustrated in Fig. 9. It is clear in this figure that the correlation between *Ta* and *Ts* weakens as the depth increases.

3.3. Discussion

Considering the low values of the error criteria (*e.g.,* RMSE) and high values of R^2, this study suggests that the STM^2 model, especially after BC, could be employed as a reliable tool for estimating *Ts* at different soil depths (Table 4–6 and Fig. 5). This finding is consistent with that of Spokas and Forcella (2009) and Perreault et al. (2013). In contrast to other soil–modeling tools, such as Hydrus1D and CoupModel, the STM^2 is very easy to use, needs very limited input data, and estimates *Ts* with very fine accuracy. Accordingly, the STM^2 can be employed as a reliable tool for *Ts* modeling purposes even by non-soil scientists, and this can be concluded as a noticeable benefit of the model, as was noted in previous studies (Perreault et al., 2013) and by its developers (Spokas and Forcella, 2009).

A previous study in northeast Iran showed that *Ts* increased at different depths, especially during warmer months of the year (Araghi et al., 2017a). Based on the results obtained in the current study, future *Ts* increases at depths of up to 100 cm are expected in this region, especially under the RCP4.5, RCP6.0, and RCP8.5 scenarios (Figs. 5-7). Using five global climate models along with ForSTem, Houle et al. (2012) demonstrated increments of 1.9–3.3 °C for the period 2070–2099 at studied forested sites in southern Quebec. For the investigated region in Iran, the current research estimated higher increments for certain RCP scenarios, with a maximum of 2.6–4.4 °C under the RCP8.5 scenario. This difference could be due to several factors. First, the choice of forested sites by Houle et al. (2012) likely contributed to differences in absorbed radiation; absorbed radiation is normally lower on bare or poorly-vegetated ground, characteristic of the current study sites. Second, the climate in Quebec (Nalley et al., 2012; Nalley et al., 2013) shares few similarities with the semi-arid to arid climate in the studied region of Iran (Araghi et al., 2018). Third, in Houle et al. (2012), five GCMs were used, while in the current study, an ensemble of 17 GCMs were employed to generate future weather data

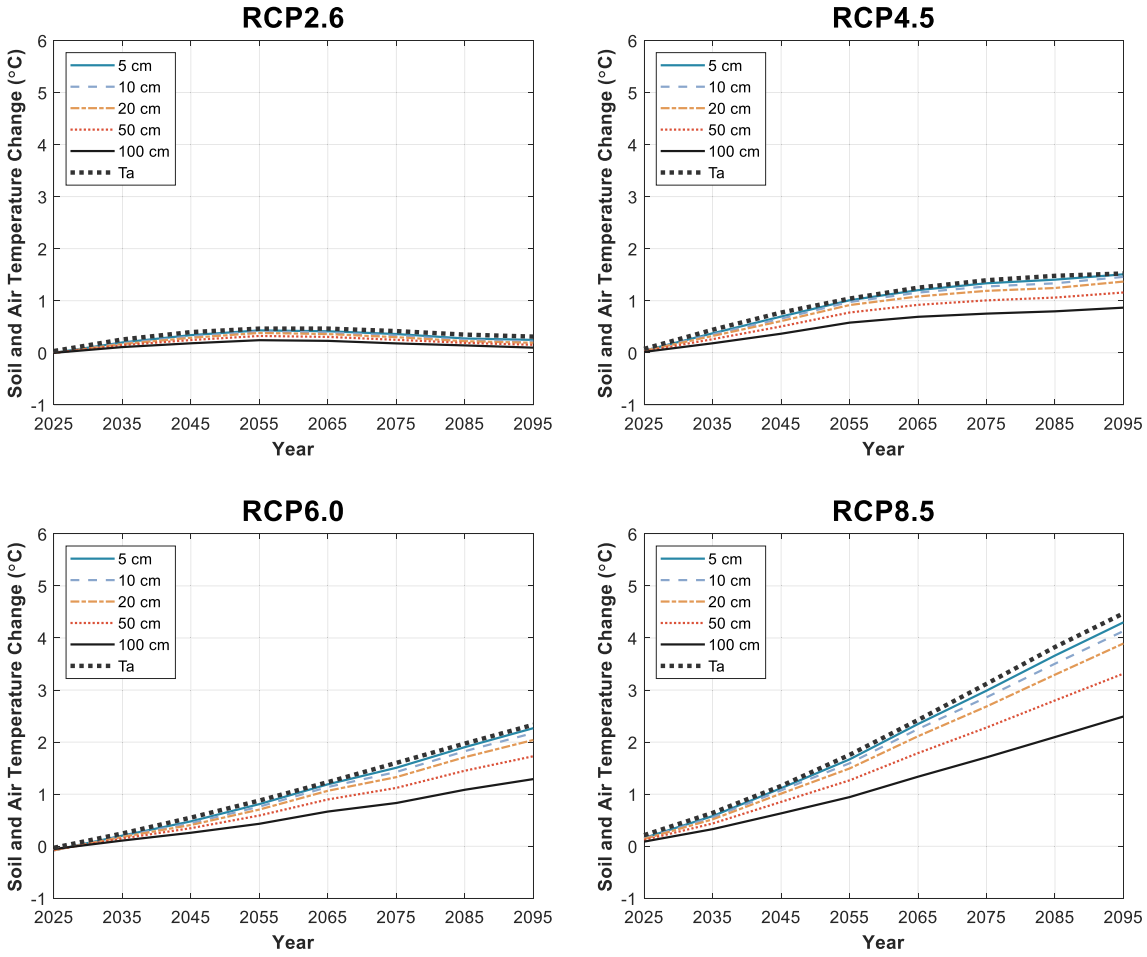

Fig. 8. Changes to future *Ts* and *Ta* projections at Mashhad station as compared to the period of 1993–2017. Determined using 17 General Circulation Models (GCMs) under four representative concentration pathways (RCPs) and the soil temperature and moisture model (STM^2).

for input into the STM^2 model. Finally, Houle et al. (2012) used For-STem, which differs from the STM^2 model used in this study, and some dissimilarities between results are likely a function of the variations in the applied models.

As in any climate change study, the existence of uncertainties in the final research results can be expected. Considering the fine performance of the STM^2 model after BC (*i.e.,* RMSE $\leq$1.6 in most cases, except at a depth of 5 cm at the Ghoochan station), it seems that most of the uncertainties in the final results of this study are due to inherent uncertainties within GCMs (Pierce et al., 2009). In most atmosphere-soil modeling tools (*e.g.,* STM^2, Noah and CLM), the amount of soil moisture is determined using *P* input data (Spokas and Forcella, 2009). The future predicted values of *P* will inherently contain higher uncertainties compared to *Ta* (Araghi et al., 2017c; Ines and Hansen, 2006), and this can be one of the most significant reasons for uncertainties in estimated future soil moisture values and *Ts*.

4. Conclusions and recommendation

In this study, future *Ts* was estimated at three weather stations in northeast Iran (Ghoochan, Gonabad, and Mashhad) using an ensemble of 17 general circulation models (GCMs) from the Coupled Model Intercomparison Project Phase 5 (CMIP5). Future *Ts* were analyzed under different representative concentration pathway (RCP) scenarios, by applying the Soil Temperature and Moisture Model (STM^2). Findings showed ranges of increments between 0.8 and 1.5 °C, 1.2–2.3 °C, and 2.4–4.4 °C in *Ts* at the studied soil depths, based on the RCP4.5, RCP6.0 and RCP8.5 scenarios, respectively. These results were similar to those found by Houle et al. (2012) in their Quebec study. An increased *Ts* may have positive effects on crop growth and development, especially during the first growth stages, such as emergence (Mavi and Tupper, 2004). However, higher *Ts* may also impact other soil processes such as the rate of nutrient and CO_2 release from soil organic matter due to microorganism activity (Melillo et al., 2002; Reth et al., 2005). Also, higher *Ts* can accelerate the evaporation rate from the soil and this can reduce the available soil water at a faster rate. Therefore, *Ts* increments can create water deficits, especially in regions with arid to semi-arid climates, similar to those investigated in this study (Araghi et al., 2018; Hillel, 1998). The approach followed in this study is widely applicable and could be employed elsewhere. *Ts* has numerous influences on soil processes and atmospheric exchange. The projections of *Ts* could be advantageous for many different areas of environmental science and climatology (*e.g.,* to study biological and chemical properties of soil, variations in seed emergence, and depth of freezing in soil), and can support the use of *Ts* as an effective tool for estimating current and future trends in microclimate, hydrology, agriculture, and other related processes. Comparing the variability of *Ts* and *Ta* in future decades, based on CMIP5 GCM models and RCP scenarios, could be an interesting topic for study in different regions worldwide. There are some soil moisture and temperature datasets for the entire globe, such as https://ismn.geo.tuwien.ac.at/en/, which would be useful for applying and testing the method proposed in this study, to compare variations of *Ts* and soil moisture in future decades. Also, improving some features, such as adding the ability to use different soil textures throughout the simulated soil profile in subsequent versions of the STM^2 model, would be useful.

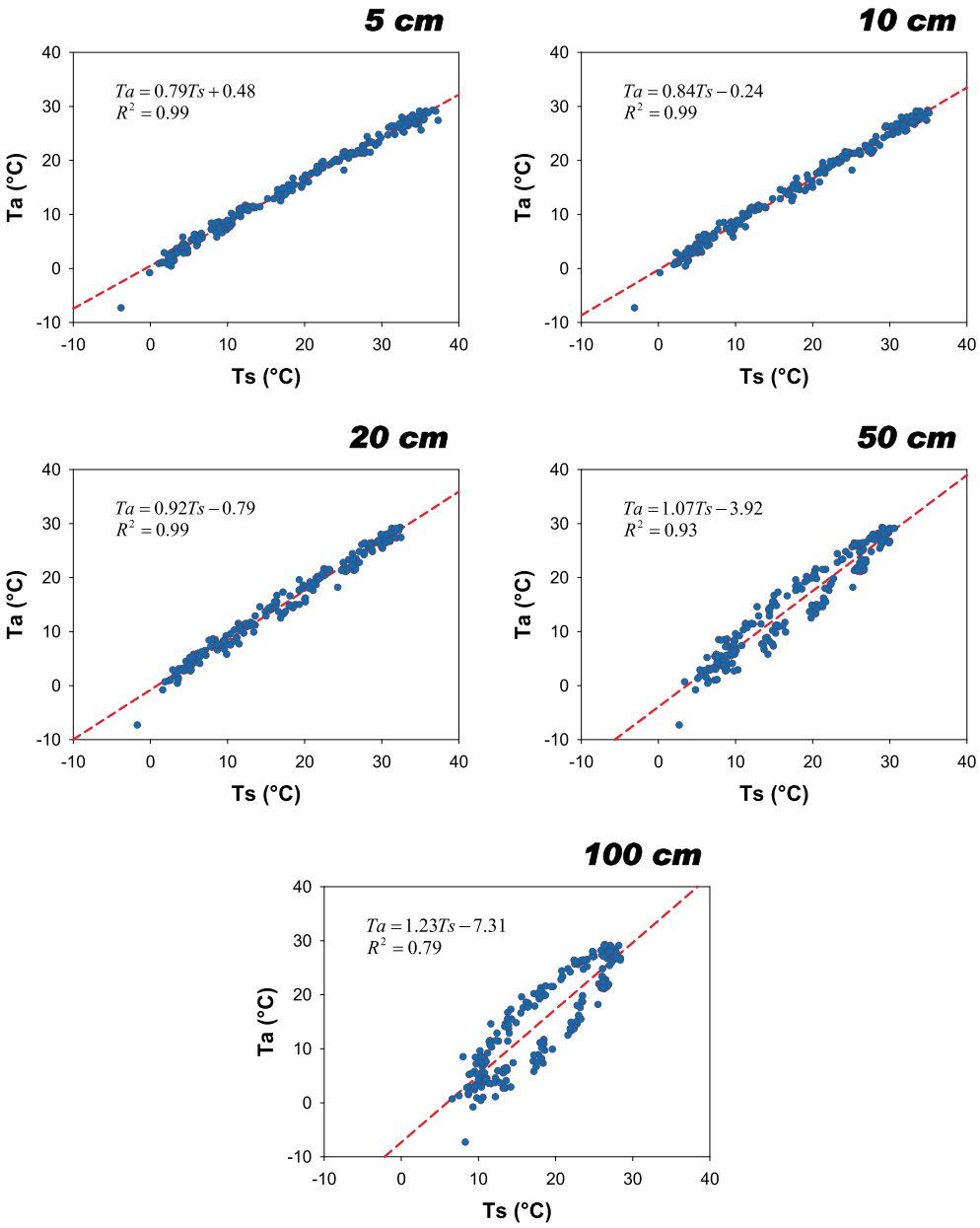

Fig. 9. Correlation between monthly *Ta* and *Ts* at different depths of soil in Mashhad station (using data from 1993 to 2017).

Acknowledgements

The authors would like to thank our reviewers whose suggestions and remarks have greatly helped us to improve the paper.

References

Allen, R.G., Pereira, L.S., Raes, D., Smith, M., 1998. Crop evapotranspiration: guidelines for computing crop water requirements. In: FAO Irrigation and Drainage Paper No. 56. FAO, Rome.

Apipattanavis, S., Podestá, G., Rajagopalan, B., Katz, R.W., 2007. A semiparametric multivariate and multisite weather generator. Water Resour. Res. 43 (11).

Araghi, A., Mousavi-Baygi, M., Adamowski, J., 2015a. Detection of trends in days with extreme temperatures in Iran from 1961 to 2010. Theor. Appl. Climatol. 125, 213–225.

Araghi, A., Mousavi-Baygi, M., Adamowski, J., Malard, J., Nalley, D., Hasheminia, S.M., 2015b. Using wavelet transforms to estimate surface temperature trends and dominant periodicities in Iran based on gridded reanalysis data. Atmos. Res. 155, 52–72.

Araghi, A., Mousavi-Baygi, M., Adamowski, J., 2017a. Detecting soil temperature trends in Northeast Iran from 1993 to 2016. Soil Tillage Res. 174, 177–192.

Araghi, A., Mousavi-Baygi, M., Adamowski, J., Martinez, C., van der Ploeg, M., 2017b. Forecasting soil temperature based on surface air temperature using a wavelet artificial neural network. Meteorol. Appl. 24 (4), 603–611.

Araghi, A., Mousavi-Baygi, M., Adamowski, J., Martinez, C., 2017c. Association between three prominent climatic teleconnections and precipitation in Iran using wavelet coherence. Int. J. Climatol. 37 (6), 2809–2830.

Araghi, A., Martinez, C., Adamowski, J., Olesen, J.E., 2018. Spatiotemporal variations of aridity in Iran using high-resolution gridded data. Int. J. Climatol. 38 (6), 2701–2717.

Batir, J.F., Hornbach, M.J., Blackwell, D.D., 2017. Ten years of measurements and modeling of soil temperature changes and their effects on permafrost in Northwestern Alaska. Glob. Planet. Chang. 148, 55–71.

Bilgili, M., 2010. Prediction of soil temperature using regression and artificial neural network models. Meteorog. Atmos. Phys. 110 (1), 59–70.

Bradford, J.B., Schlaepfer, D.R., Lauenroth, W.K., Yackulic, C.B., Duniway, M., Hall, S., Jia, G., Jamiyansharav, K., Munson, S.M., Wilson, S.D., Tietjen, B., 2017. Future soil moisture and temperature extremes imply expanding suitability for rainfed agriculture in temperate drylands. Sci. Rep. 7 (1), 12923.

Brutsaert, W., 2010. Hydrology, an Introduction, 1st ed. Cambridge University Press, New York.

Chatterjee, S., Hadi, A.S., 2012. Regression Analysis by Example, 5th ed. John Wiley & Sons Inc., Hoboken, NJ.

Collier, M.A.J., Stephen J; Rotstayn, Leon D; Wong, K K H; Dravitzki, S M; Moeseneder, C; Hamalainen, C; Syktus, J I; Suppiah, Ramasamy; Antony, Joseph; El Zein, Ahmed; Atif, Muhammad, 2011. The CSIRO-Mk 3.6.0 Atmosphere-Ocean GCM: Participation in CMIP5 and Data Publication, MODSIM vol. 2011, Perth.

Collins, W.J., Bellouin, N., Doutriaux-Boucher, M., Gedney, N., Halloran, P., Hinton, T.,

Hughes, J., Jones, C.D., Joshi, M., Liddicoat, S., Martin, G., O'Connor, F., Rae, J., Senior, C., Sitch, S., Totterdell, I., Wiltshire, A., Woodward, S., 2011. Development and evaluation of an Earth-System model – HadGEM2. Geosci. Model Dev. 4 (4), 1051–1075.

Crowther, T.W., Todd-Brown, K.E.O., Rowe, C.W., Wieder, W.R., Carey, J.C., Machmuller, M.B., Snoek, B.L., Fang, S., Zhou, G., Allison, S.D., Blair, J.M., Bridgham, S.D., Burton, A.J., Carrillo, Y., Reich, P.B., Clark, J.S., Classen, A.T., Dijkstra, F.A., Elberling, B., Emmett, B.A., Estiarte, M., Frey, S.D., Guo, J., Harte, J., Jiang, L., Johnson, B.R., Kröel-Dulay, G., Larsen, K.S., Laudon, H., Lavallee, J.M., Luo, Y., Lupascu, M., Ma, L.N., Marhan, S., Michelsen, A., Mohan, J., Niu, S., Pendall, E., Peñuelas, J., Pfeifer-Meister, L., Poll, C., Reinsch, S., Reynolds, L.L., Schmidt, I.K., Sistla, S., Sokol, N.W., Templer, P.H., Treseder, K.K., Welker, J.M., Bradford, M.A., 2016. Quantifying global soil carbon losses in response to warming. Nature 540, 104–110.

Davidson, E.A., Janssens, I.A., 2006. Temperature sensitivity of soil carbon decomposition and feedbacks to climate change. Nature 440, 165–173.

Donner, L.J., Wyman, B.L., Hemler, R.S., Horowitz, L.W., Ming, Y., Zhao, M., Golaz, J.-C., Ginoux, P., Lin, S.-J., Schwarzkopf, M.D., Austin, J., Alaka, G., Cooke, W.F., Delworth, T.L., Freidenreich, S.M., Gordon, C.T., Griffies, S.M., Held, I.M., Hurlin, W.J., Klein, S.A., Knutson, T.R., Langenhorst, A.R., Lee, H.-C., Lin, Y., Magi, B.I., Malyshev, S.L., Milly, P.C.D., Naik, V., Nath, M.J., Pincus, R., Ploshay, J.J., Ramaswamy, V., Seman, C.J., Shevliakova, E., Sirutis, J.J., Stern, W.F., Stouffer, R.J., Wilson, R.J., Winton, M., Wittenberg, A.T., Zeng, F., 2011. The dynamical core, physical parameterizations, and basic simulation characteristics of the atmospheric component AM3 of the GFDL global coupled model CM3. J. Clim. 24 (13), 3484–3519.

Dufresne, J.-L., Foujols, M.-A., Denvil, S., Caubel, A., Marti, O., Aumont, O., Balkanski, Y., Bekki, S., Bellenger, H., Benshila, R., Bony, S., Bopp, L., Braconnot, P., Brockmann, P., Cadule, P., Cheruy, F., Codron, F., Cozic, A., Cugnet, D., de Noblet, N., Duvel, J.-P., Ethé, C., Fairhead, L., Fichefet, T., Flavoni, S., Friedlingstein, P., Grandpeix, J.-Y., Guez, L., Guilyardi, E., Hauglustaine, D., Hourdin, F., Idelkadi, A., Ghattas, J., Joussaume, S., Kageyama, M., Krinner, G., Labetoulle, S., Lahellec, A., Lefebvre, M.-P., Lefevre, F., Levy, C., Li, Z.X., Lloyd, J., Lott, F., Madec, G., Mancip, M., Marchand, M., Masson, S., Meurdesoif, Y., Mignot, J., Musat, I., Parouty, S., Polcher, J., Rio, C., Schulz, M., Swingedouw, D., Szopa, S., Talandier, C., Terray, P., Viovy, N., Vuichard, N., 2013. Climate change projections using the IPSL-CM5 Earth System Model: from CMIP3 to CMIP5. Clim. Dyn. 40 (9–10), 2123–2165.

Dunne, J.P., John, J.G., Adcroft, A.J., Griffies, S.M., Hallberg, R.W., Shevliakova, E., Stouffer, R.J., Cooke, W., Dunne, K.A., Harrison, M.J., Krasting, J.P., Malyshev, S.L., Milly, P.C.D., Phillipps, P.J., Sentman, L.T., Samuels, B.L., Spelman, M.J., Winton, M., Wittenberg, A.T., Zadeh, N., 2012. GFDL's ESM2 Global Coupled Climate–Carbon Earth System Models. Part I: physical formulation and baseline simulation characteristics. J. Clim. 25 (19), 6646–6665.

Fang, X., Luo, S., Lyu, S., 2019. Observed soil temperature trends associated with climate change in the Tibetan Plateau, 1960–2014. Theor. Appl. Climatol. 135 (1–2), 169–181.

Fick, S.E., Hijmans, R.J., 2017. WorldClim 2: new 1-km spatial resolution climate surfaces for global land areas. Int. J. Climatol. 37 (12), 4302–4315.

Flerchinger, G.N., Kustas, W.P., Weltz, M.A., 1998. Simulating surface energy fluxes and radiometric surface temperatures for two arid vegetation communities using the SHAW model. J. Appl. Meteorol. 37 (5), 449–460.

Hillel, D., 1998. Environmental Soil Physics. Academic Press, San Diego.

Houle, D., Bouffard, A., Duchesne, L., Logan, T., Harvey, R., 2012. Projections of future soil temperature and water content for three southern Quebec forested sites. J. Clim. 25 (21), 7690–7701.

Hyndman, R.J., Koehler, A.B., 2006. Another look at measures of forecast accuracy. Int. J. Forecast. 22, 678–688.

Ines, A.V.M., Hansen, J.W., 2006. Bias correction of daily GCM rainfall for crop simulation studies. Agric. For. Meteorol. 138 (1), 44–53.

IPCC, 2013. Fifth Assessment Report of the Intergovernmental Panel on Climate Change. Intergovernmental Panel on Climate Change, NY, USA.

Jones, P.G., Thornton, P.K., 2000. MarkSim: software to generate daily weather data for Latin America and Africa. Agron. J. 92 (3), 445–453.

Jones, P.G., Thornton, P.K., 2013. Generating downscaled weather data from a suite of climate models for agricultural modelling applications. Agric. Syst. 114, 1–5.

Jones, P.G., Thornton, P.K., 2015. Representative soil profiles for the Harmonized World Soil Database at different spatial resolutions for agricultural modelling applications. Agric. Syst. 139, 93–99.

Jungqvist, G., Oni, S.K., Teutschbein, C., Futter, M.N., 2014. Effect of climate change on soil temperature in Swedish boreal forests. PLoS One 9 (4).

Kemp, P.R., Cornelius, J.M., Reynolds, J.F., 1992. A simple model for predicting soil temperatures in desert ecosystems. Soil Sci. 153 (4), 280–287.

Kirkevag, A., Iversen, T., Seland, O., Debernard, J.B., Storelvmo, T., Kristjansson, J.E., 2008. Aerosol-cloud-climate interactions in the climate model CAM-Oslo. Tellus A 60 (3), 492–512.

Knight, J.H., Minasny, B., McBratney, A.B., Koen, T.B., Murphy, B.W., 2018. Soil temperature increase in eastern Australia for the past 50 years. Geoderma 313, 241–249 Supplement C.

Leander, R., Buishand, T.A., 2007. Resampling of regional climate model output for the simulation of extreme river flows. J. Hydrol. 332 (3), 487–496.

Lenderink, G., Buishand, A., van Deursen, W., 2007. Estimates of future discharges of the river Rhine using two scenario methodologies: direct versus delta approach. Hydrol. Earth Syst. Sci. 11 (3), 1145–1159.

Mavi, H.S., Tupper, G.J., 2004. Agrometeorology, Principles and Applications of Climate Studies in Agriculture. Food Products Press.

Meinshausen, M., Smith, S.J., Calvin, K., Daniel, J.S., Kainuma, M.L.T., Lamarque, J.F., Matsumoto, K., Montzka, S.A., Raper, S.C.B., Riahi, K., Thomson, A., Velders, G.J.M., van Vuuren, D.P.P., 2011. The RCP greenhouse gas concentrations and their extensions from 1765 to 2300. Clim. Chang. 109 (1), 213–241.

Melillo, J.M., Steudler, P.A., Aber, J.D., Newkirk, K., Lux, H., Bowles, F.P., Catricala, C., Magill, A., Ahrens, T., Morrisseau, S., 2002. Soil warming and carbon-cycle feedbacks to the climate system. Science 298 (5601), 2173–2176.

Mellander, P.-E., Löfvenius, M.O., Laudon, H., 2007. Climate change impact on snow and soil temperature in boreal scots pine stands. Clim. Chang. 85 (1), 179–193.

Moss, R.H., Edmonds, J.A., Hibbard, K.A., Manning, M.R., Rose, S.K., van Vuuren, D.P., Carter, T.R., Emori, S., Kainuma, M., Kram, T., Meehl, G.A., Mitchell, J.F.B., Nakicenovic, N., Riahi, K., Smith, S.J., Stouffer, R.J., Thomson, A.M., Weyant, J.P., Wilbanks, T.J., 2010. The next generation of scenarios for climate change research and assessment. Nature 463, 747–756.

Najafimoud, M.H., Alizadeh, A., Mohamadian, A., Mousavi, J., 2008. Investigation of relationship between air and soil temperature at different depths and estimation of the freezing depth (case study: Khorasan Razavi). Journal of Water and Soil 22 (2), 456–466.

Nalley, D., Adamowski, J., Khalil, B., 2012. Using discrete wavelet transforms to analyze trends in streamflow and precipitation in Quebec and Ontario (1954–2008). J. Hydrol. 475, 204–228.

Nalley, D., Adamowski, J., Khalil, B., Ozga-Zielinski, B., 2013. Trend detection in surface air temperature in Ontario and Quebec, Canada during 1967–2006 using the discrete wavelet transform. Atmos. Res. 132–133 (0), 375–398.

Paymard, P., Bannayan, M., Haghighi, R.S., 2018. Analysis of the climate change effect on wheat production systems and investigate the potential of management strategies. Nat. Hazards 91 (3), 1237–1255.

Peleg, N., Fatichi, S., Paschalis, A., Molnar, P., Burlando, P., 2017. An advanced stochastic weather generator for simulating 2-D high-resolution climate variables. J. Adv. Model. Earth Syst. 9 (3), 1595–1627.

Perreault, S., Chokmani, K., Nolin, M.C., Bourgeois, G., 2013. Validation of a soil temperature and moisture model in Southern Quebec, Canada. Soil Sci. Soc. Am. J. 77, 606–617.

Piani, C., Weedon, G.P., Best, M., Gomes, S.M., Viterbo, P., Hagemann, S., Haerter, J.O., 2010. Statistical bias correction of global simulated daily precipitation and temperature for the application of hydrological models. J. Hydrol. 395 (3), 199–215.

Pierce, D.W., Barnett, T.P., Santer, B.D., Gleckler, P.J., 2009. Selecting global climate models for regional climate change studies. Proc. Natl. Acad. Sci. 106 (21), 8441–8446.

Qian, B., Gregorich, E.G., Gameda, S., Hopkins, D.W., Wang, X.L., 2011. Observed soil temperature trends associated with climate change in Canada. J. Geophys. Res. Atmos. 116 (2).

Reth, S., Reichstein, M., Falge, E., 2005. The effect of soil water content, soil temperature, soil pH-value and the root mass on soil CO_2 efflux – a modified model. Plant Soil 268 (1), 21–33.

Richardson, C.W., 1981. Stochastic simulation of daily precipitation, temperature, and solar radiation. Water Resour. Res. 17 (1), 182–190.

Rogelj, J., Meinshausen, M., Knutti, R., 2012. Global warming under old and new scenarios using IPCC climate sensitivity range estimates. Nat. Clim. Chang. 2, 248–253.

Sanikhani, H., Deo, R.C., Yaseen, Z.M., Eray, O., Kisi, O., 2018. Non-tuned data intelligent model for soil temperature estimation: A new approach. Geoderma 330, 52–64.

Schmidt, G.A., Ruedy, R., Hansen, J.E., Aleinov, I., Bell, N., Bauer, M., Bauer, S., Cairns, B., Canuto, V., Cheng, Y., Genio, A.D., Faluvegi, G., Friend, A.D., Hall, T.M., Hu, Y., Kelley, M., Kiang, N.Y., Koch, D., Lacis, A.A., Lerner, J., Lo, K.K., Miller, R.L., Nazarenko, L., Oinas, V., Perlwitz, J., Perlwitz, J., Rind, D., Romanou, A., Russell, G.L., Sato, M., Shindell, D.T., Stone, P.H., Sun, S., Tausnev, N., Thresher, D., Yao, M.-S., 2006. Present-day atmospheric simulations using GISS ModelE: comparison to in situ, satellite, and reanalysis data. J. Clim. 19 (2), 153–192.

Seland, O., Iversen, T., Kirkevag, A., Storelvmo, T., 2008. Aerosol-climate interactions in the CAM-Oslo atmospheric GCM and investigation of associated basic shortcomings. Tellus A 60 (3), 459–491.

Šimůnek, J., van Genuchten, M.T., Šejna, M., 2008. Development and applications of the HYDRUS and STANMOD software packages and related codes. Vadose Zone J. 7 (2), 587–600.

Song, Z., Qiao, F., Song, Y., 2012. Response of the Equatorial Basin-Wide SST to Non-breaking Surface Wave-Induced Mixing in a Climate Model: An Amendment to Tropical Bias. vol. 117(C11).

Spokas, K., Forcella, F., 2009. Software tools for weed seed germination modeling. Weed Sci. 57 (2), 216–227.

Taylor, K.E., Stouffer, R.J., Meehl, G.A., 2012. An overview of CMIP5 and the experiment design. Bull. Am. Meteorol. Soc. 93 (4), 485–498.

Teutschbein, C., Seibert, J., 2012. Bias correction of regional climate model simulations for hydrological climate-change impact studies: review and evaluation of different methods. J. Hydrol. 456-457, 12–29.

Watanabe, M., Suzuki, T., O'ishi, R., Komuro, Y., Watanabe, S., Emori, S., Takemura, T., Chikira, M., Ogura, T., Sekiguchi, M., Takata, K., Yamazaki, D., Yokohata, T., Nozawa, T., Hasumi, H., Tatebe, H., Kimoto, M., 2010. Improved climate simulation by MIROC5: mean states, variability, and climate sensitivity. J. Clim. 23 (23), 6312–6335.

Watanabe, S., Hajima, T., Sudo, K., Nagashima, T., Takemura, T., Okajima, H., Nozawa, T., Kawase, H., Abe, M., Yokohata, T., Ise, T., Sato, H., Kato, E., Takata, K., Emori, S., Kawamiya, M., 2011. MIROC-ESM 2010: model description and basic results of CMIP5-20c3m experiments. Geosci. Model Dev. 4 (4), 845–872.

Wilks, D.S., 2011. Statistical Methods in the Atmospheric Science. International Geophysics, 3rd ed. Academic Press, USA.

Wisser, D., Marchenko, S., Talbot, J., Treat, C., Frolking, S., 2011. Soil temperature response to 21st century global warming: the role of and some implications for peat

carbon in thawing permafrost soils in North America. Earth Syst. Dynam. 2 (1), 121–138.
WMO, 2008. Guide to Meteorological Instruments and Methods of Observation, 7th ed. World Meteorological Organization, Geneva.
Wu, T., 2012. A mass-flux cumulus parameterization scheme for large-scale models: description and test with observations. Clim. Dyn. 38 (3–4), 725–744.
Wu, W., Tang, X.P., Guo, N.J., Yang, C., Liu, H.B., Shang, Y.F., 2013. Spatiotemporal modeling of monthly soil temperature using artificial neural networks. Theor. Appl. Climatol. 113 (3–4), 481–494.
Yukimoto, S., Adachi, Y., Hosaka, M., Sakami, T., Yoshimura, H., Hirabara, M., Tanaka, T.Y., Shindo, E., Tsujino, H., Deushi, M., Mizuta, R., Yabu, S., Obata, A., Nakano, H., Koshiro, T., Ose, T., Kitoh, A., 2012. A new global climate model of the meteorological research institute: MRI-CGCM3 -model description and basic performance. J. Meteorol. Soc. Jpn. 90A, 23–64.
Zhang, Y., Chen, W., Smith, S.L., Riseborough, D.W., Cihlar, J., 2005. Soil temperature in Canada during the twentieth century: complex responses to atmospheric climate change. J. Geophys. Res. Atmos. 110 (D3).
Zhang, H., Wang, E., Zhou, D., Luo, Z., Zhang, Z., 2016. Rising soil temperature in China and its potential ecological impact. Sci. Rep. 6, 1–8.